Mechanism of Cu_A assembly

Luciano A.Abriata[1], Lucia Banci[2], Ivano Bertini[2,*], Simone Ciofi-Baffoni[2], Petros Gkazonis[2,3], Georgios A. Spyroulias[3], Alejandro J. Vila[1], Shenlin Wang[2]

Supplementary Data

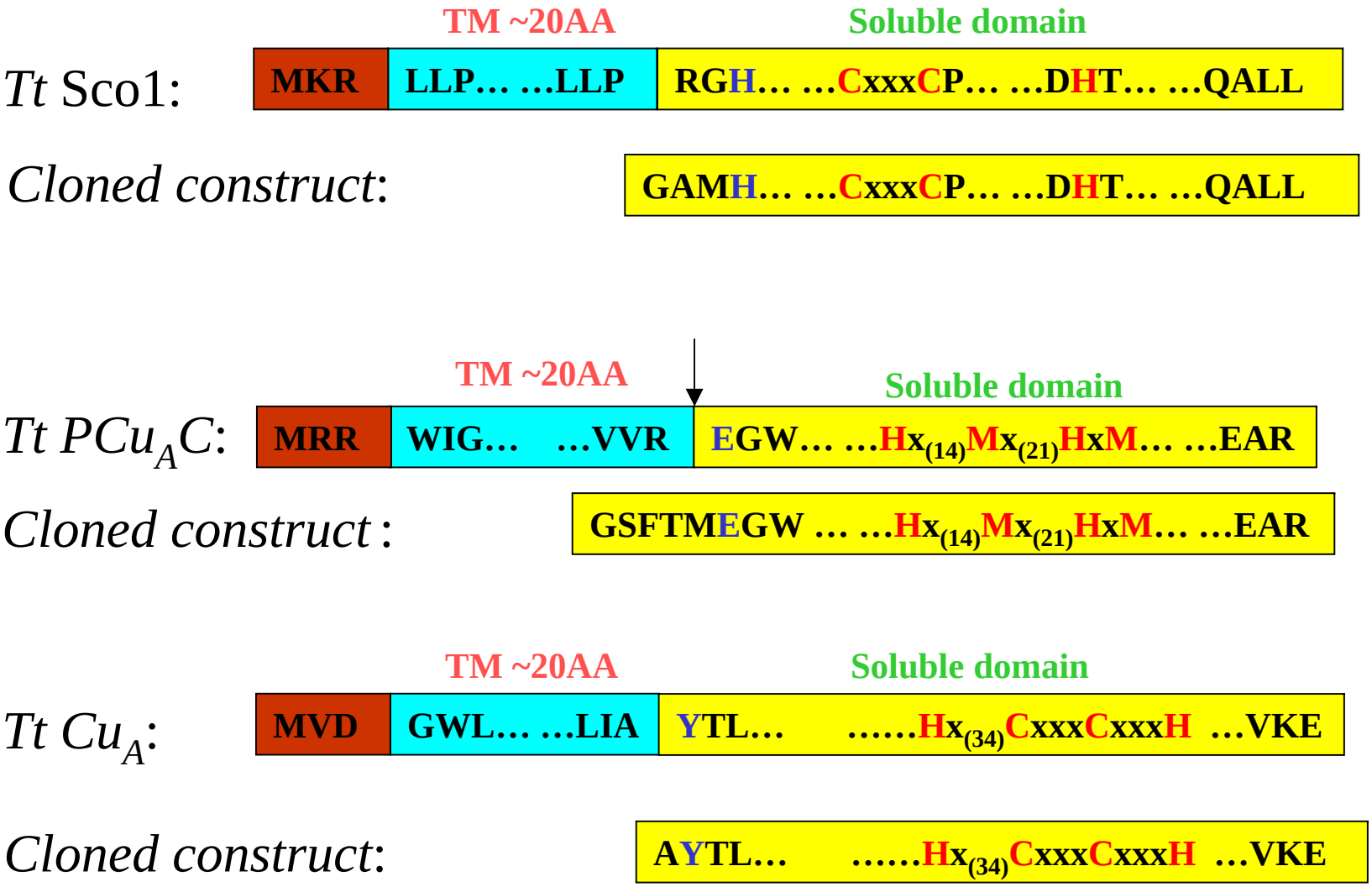

Supplementary Figure 1. Schematic representation of the full length proteins and cloned constructs of *Tt* Sco1, *Tt* PCu_AC and *Tt* Cu_A. The positions of the transmembrane helical domains (TM) for the three proteins are shown in cyan, while soluble and cloned domains in yellow. The peptide leader sequence of *Tt* PCu_AC predicted by software SignalP is indicated by an arrow. The metal ligands are indicated in red within the metal binding pattern.

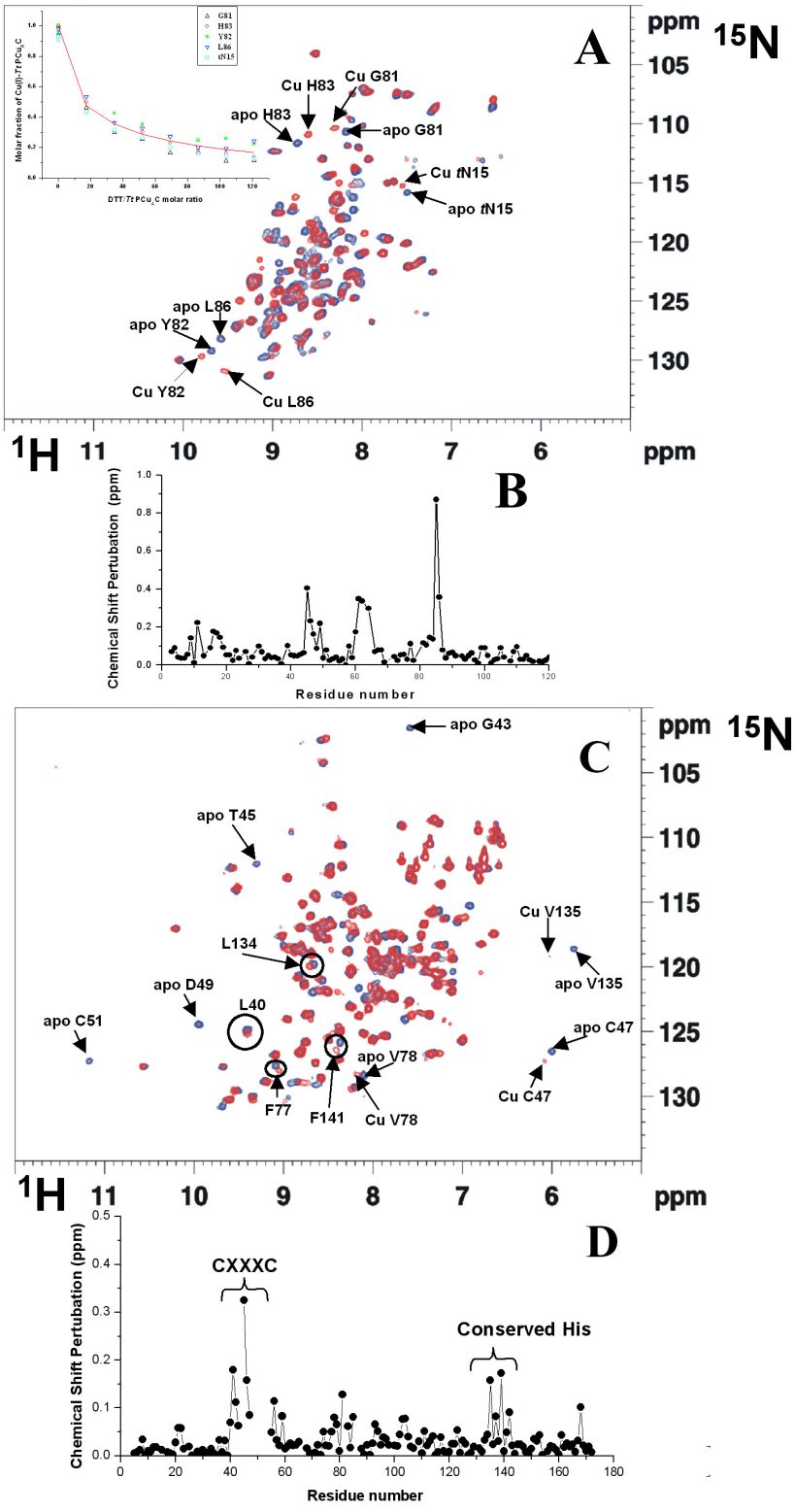

Supplementary Figure 2. Binding of Cu(I) to apo-*Tt* PCu_AC and to apo-*Tt* Sco1. (A) ^1H,^{15}N HSQC spectra of apo-*Tt* PCu_AC (blue) and Cu(I)-*Tt* PCu_AC (red). The most affected NH crosspeaks upon titration of the apo-protein with Cu(I) are indicated. In the inset, the molar fraction of Cu(I)-*Tt* PCu_AC as a function of DTT/*Tt* PCu_AC ratio is plotted. (B) Chemical shift perturbation of the NH moieties ($\Delta_{avg}(HN) = \{[(\Delta H)^2 + (\Delta N/5)^2]/2\}^{1/2}$, where ΔH and ΔN are the chemical shift differences for ^1H and ^{15}N, respectively) of apo-*Tt* PCu_AC upon addition of Cu(I). Metal binding residues or pattern are also indicated. (C) ^1H,^{15}N HSQC spectra of apo-*Tt* Sco1 (blue) and Cu(I)-*Tt* Sco1 (red). The most affected crosspeaks upon titration of the apo-protein with Cu(I) are indicated. (D) Chemical shift perturbation of the NH moieties of apo-*Tt* Sco1 upon addition with Cu(I). Metal binding residues or pattern are also indicated.

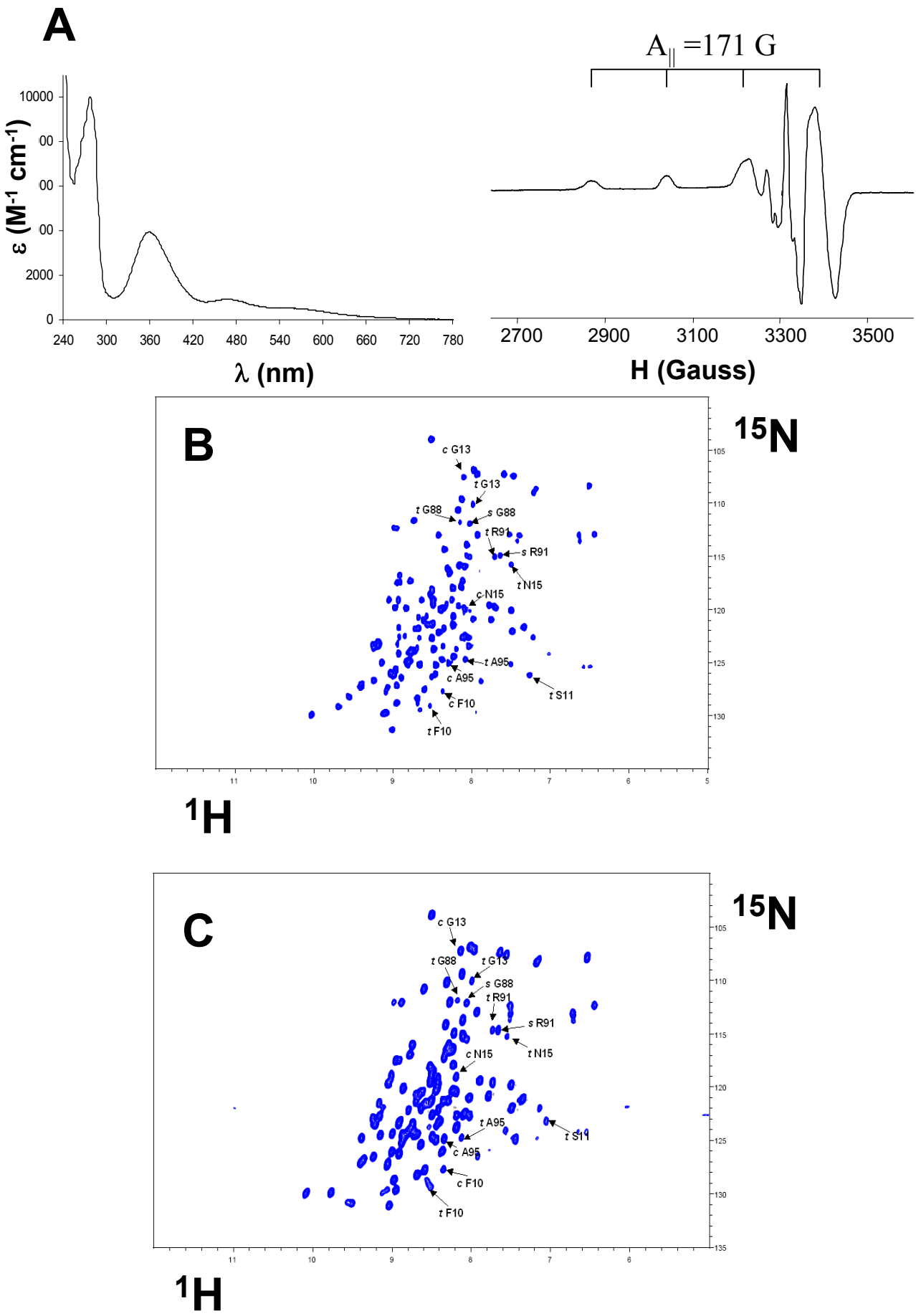

Supplementary Figure 3. Electronic and EPR spectra of Cu(II)-*Tt* Sco1 (A) and $^{1}H,^{15}N$ HSQC spectra of apo-*Tt* PCu_AC (B) and Cu(I)-*Tt* PCu_AC (C). The X-band EPR of Cu(II)-*Tt* Sco1 gives a nearly axial copper spectrum with $g_{\|}$ = 2.15, $g_{\perp}$ = 2.03. NMR resonances corresponding to the residues involved in the *cis/trans* isomerization of Pro14 are indicated with *c* and *t* lettering.

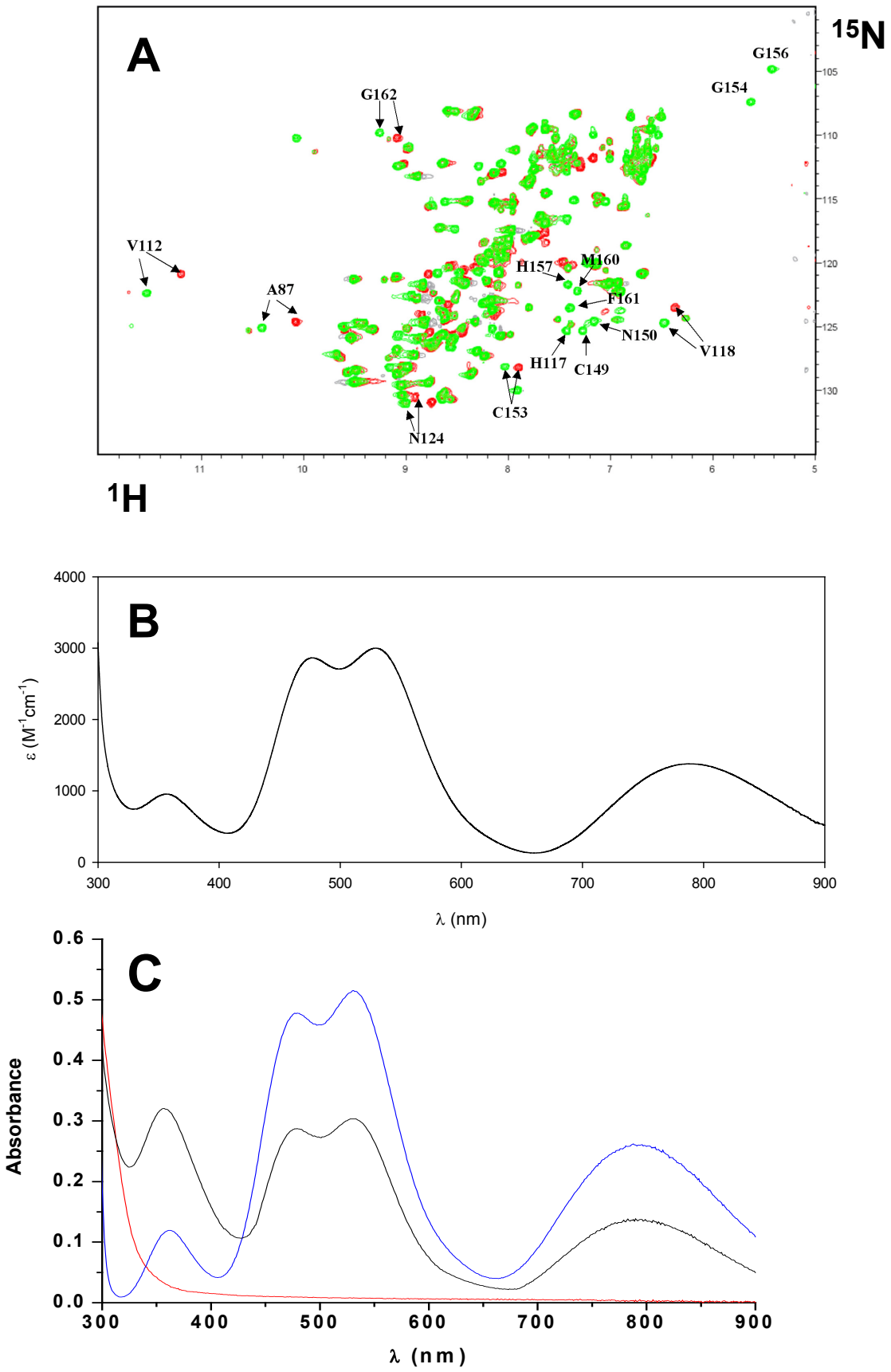

Supplementary Figure 4. Effect of copper(I) addition to apo-*Tt* Cu_A and electronic spectra of *Tt* Cu_A:Cu(I)-*Tt* PCu_AC mixture (A) ^1H,^{15}N HSQC spectra of apo-*Tt* Cu_A (red) and $Cu(I)_2$-*Tt* Cu_A (green) and (B) UV-vis spectrum of Cu(II),Cu(I)-*Tt* Cu_A obtained after air exposure of $Cu(I)_2$-*Tt* Cu_A. (C) Electronic spectra of a 1:2 mixture of *Tt* Cu_A:Cu(I)-*Tt* PCu_AC before (red) and after air exposure (black) compared to that of Cu(II),Cu(I)-*Tt* Cu_A (blue).

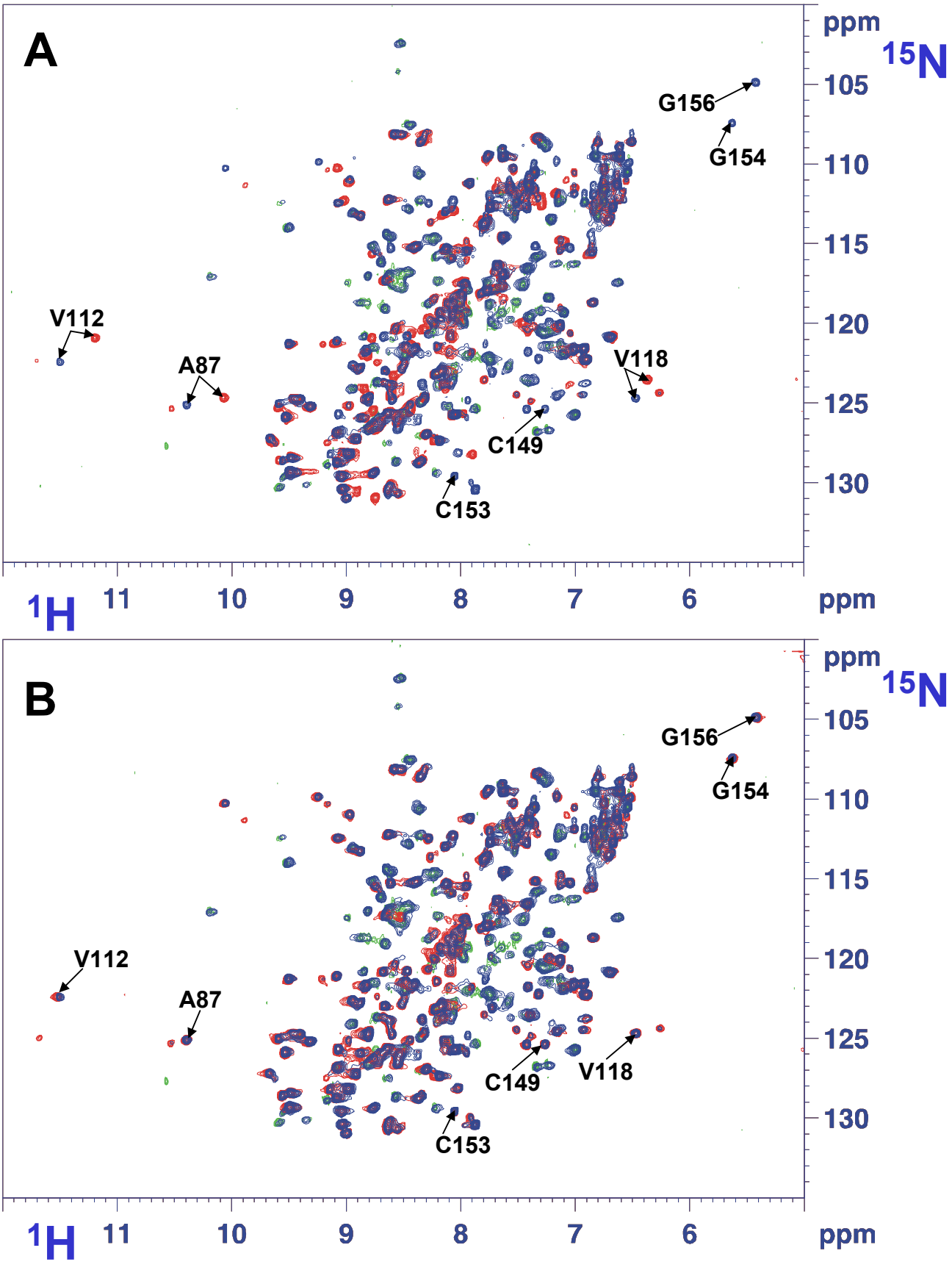

Supplementary Figure 5. Formation of Cu(I)$_2$-*Tt* Cu$_A$ in the presence of Cu(II)-*Tt* Sco1 and Cu(I)-*Tt* PCu$_A$C followed by NMR. (A) Overlay of the ^{1}H-^{15}N HSQC spectra of a 1:1:2 mixture of ^{15}N apo-*Tt* Cu$_A$:^{15}N Cu(II)-*Tt* Sco1: unlabeled Cu(I)-*Tt* PCu$_A$C (blue), ^{15}N Cu(II)-*Tt* Sco1 (green) and ^{15}N apo-*Tt* Cu$_A$ (red). (B) Overlay of the ^{1}H-^{15}N HSQC spectra of a 1:1:2 mixture of ^{15}N apo-*Tt* Cu$_A$: ^{15}N Cu(II)-*Tt* Sco1: unlabelled Cu(I)-*Tt* PCu$_A$C (blue), ^{15}N Cu(II)-*Tt* Sco1 (green) and ^{15}N Cu(I)$_2$-*Tt* Cu$_A$ (red). The typical NH resonances indicative of the formation of Cu(I)$_2$-*Tt* Cu$_A$ form are shown, thus discarding a possible mechanism involving a concerted action of both Cu(II)-*Tt* Sco1 and Cu(I)-*Tt* PCu$_A$C to give rise to a mixed valence, oxizided Cu$_A$ site.

Table S1 Statistical analysis of the energy minimized family of conformers of apo-*Tt* PCu_AC (*trans* and *cis* conformation).

	apo-*Tt* PCu_AC (*trans* conformation)	apo-*Tt* PCu_AC (*cis* conformation)
NMR distance and dihedral constraints		
Distance constraints		
Total NOE	1817	1804
Intra-residue	440	451
Inter-residue	1377	1353
Sequential ($\|i-j\|=1$)	505	528
Medium-range ($\|i-j\|<4$)	165	169
Long-range ($\|i-j\|>5$)	707	656
Intermolecular	0	0
Hydrogen bonds	0	0
Total dihedral angle restraints		
ϕ	61	61
ψ	62	62
Structure statistics		
Violations (mean and s.d.)		
Distance constraints (Å)	0.076 ± 0.007	0.075 ± 0.008
Dihedral angle constraints (º)	0.37 ± 0.04	0.23 ± 0.02
Max. dihedral angle violation (º)	9.50	10.50
Max. distance constraint violation (Å)	0.27	0.29
Deviations from idealized geometry		
Bond lengths (Å)	0.0090 ± 0.0002	0.0090 ± 0.0002
Bond angles (º)	2.20 ± 0.03	2.22 ± 0.03
Impropers (º)	0.11 ± 0.02	0.11 ± 0.03
Average pairwise r.m.s. deviation** (Å)		
Heavy	1.19 ± 0.09	1.17 ± 0.12
Backbone	0.74 ± 0.08	0.73 ± 0.12

** Pairwise r.m.s. deviation was calculated among 30 refined structures.

Table S2 Statistical analysis of the energy minimized family of conformers of Cu(I)-*Tt* PCu_AC (*trans* and *cis* conformation).

	Cu(I)-*Tt* PCu_AC (*trans* conformation)	Cu(I)-*Tt* PCu_AC (*cis* conformation)
NMR distance and dihedral constraints		
Distance constraints		
Total NOE	1773	1852
Intra-residue	382	416
Inter-residue	1391	1436
Sequential ($\|i - j\| = 1$)	535	539
Medium-range ($\|i - j\| < 4$)	159	171
Long-range ($\|i - j\| > 5$)	697	726
Intermolecular	0	0
Hydrogen bonds	0	0
Total dihedral angle restraints		
ϕ	61	61
ψ	62	62
Structure statistics		
Violations (mean and s.d.)		
Distance constraints (Å)	0.072 ± 0.007	0.073 ± 0.006
Dihedral angle constraints (º)	0.23 ± 0.03	0.24 ± 0.02
Max. dihedral angle violation (º)	11.30	9.25
Max. distance constraint violation (Å)	0.19	0.19
Deviations from idealized geometry		
Bond lengths (Å)	0.010 ± 0.003	0.010 ± 0.002
Bond angles (º)	2.31 ± 0.03	2.33 ± 0.02
Impropers (º)	0.10 ± 0.02	0.091 ± 0.002
Average pairwise r.m.s. deviation** (Å)		
Heavy	1.17 ± 0.08	1.18 ± 0.08
Backbone	0.69 ± 0.09	0.71 ± 0.08

** Pairwise r.m.s. deviation was calculated among 30 refined structures.

Table S3 Statistical analysis of the energy minimized family of conformers of apo-*Tt* Sco1.

	apo-*Tt* Sco1
NMR distance and dihedral constraints	
Distance constraints	
Total NOE	2156
Intra-residue	636
Inter-residue	1520
Sequential ($\|i - j\| = 1$)	607
Medium-range ($\|i - j\| < 4$)	352
Long-range ($\|i - j\| > 5$)	561
Intermolecular	0
Hydrogen bonds	0
Total dihedral angle restraints	
ϕ	84
ψ	93
Structure statistics	
Violations (mean and s.d.)	
Distance constraints (Å)	0.073 ± 0.007
Dihedral angle constraints (º)	0.35 ± 0.03
Max. dihedral angle violation (º)	9.34
Max. distance constraint violation (Å)	0.27
Deviations from idealized geometry	
Bond lengths (Å)	0.0093 ± 0.0001
Bond angles (º)	2.17 ± 0.03
Impropers (º)	1.07 ± 0.22
Average pairwise r.m.s. deviation** (Å)	
Heavy	1.51 ± 0.24
Backbone	0.99 ± 0.25

** Pairwise r.m.s. deviation was calculated among 30 refined structures.

Supplementary methods

Bioinformatic tools ---- STRING program (http://string.embl.de) was used to identify the *Thermos thermopiles* Sco neighboring genes. Prediction of transmembrane helices, of membrane topology and of signal peptide cleavage sites were obtained by using the HMMTOP, TMPRED and SignalP programs available from http://www.expasy.ch web site.

Samples preparation ---- *Tt* Sco1, *Tt* Cu_A and *Tt* PCu_AC were here expressed in *E. coli* to high levels, and purified to homogeneity in the apo forms, as determined by ESI mass spectrometry. Treatment of *Tt* Sco1 with DTNB did not reveal the presence of exposed thiol groups, even in the presence of 7.3 M guanidinium chloride, suggesting that the cysteine thiols were fully oxidized in the aerobic conditions. No Cys residues are present in the *Tt* PCu_AC amino acid sequence.

Tt PCu_AC and *Tt* Sco1 were expressed in *E. coli* BL21-Gold (DE3) cells (Stratagene), which were grown in LB and minimal medium [$(^{15}NH_4)_2SO_4$ and/or [^{13}C]-glucose] for the production of labeled samples. Purification of *Tt* PCu_AC was performed by using a HiTrap chelating HP column (Amersham Pharmacia Biosciences) charged with Ni(II). His-GST tag was then cleaved with AcTEV, and separated from the C-terminal domain with a second purification step. After this purification, the protein preparations showed a single component by SDS-PAGE. The Cu(I) metallated form was obtained by addition of stoichiometric amounts of the metal ion, $(Cu(I)(CH_3CN)_4)PF_6$) to diluted protein solutions in 50 mM phosphate buffer at pH 7.2 and 1 mM ascorbate, followed by protein concentration under nitrogen atmosphere. *Tt* Sco1 was purified from the cell lysate by chromatography on a Nickel-NTA affinity column. The poly-His tag was cleaved with rTEV protease and a second step of affinity chromatography was performed to remove the His tag. Protein expression and purification were monitored by sodium dodecyl phosphate-polyacrylamide gel electrophoresis in 14% polyacrylamide gels stained with Coomassie brilliant blue R-250. Right after purification, the protein was stored in 50 mM Tris pH 8, 200 mM NaCl, 10% glycerol, at 4°C. Before use, apo-*Tt* Sco1 samples were reduced with 5mM DTT for 30 minutes and excess DTT was

removed by desalting chromatography, and buffer changed to 100 mM potassium phosphate pH 7, with 1 mM DTT when appropriate. All these manipulations were performed under anaerobic conditions. Binding of Cu(I) and Cu(II) ions to apo-*Tt* Sco1 was followed by NMR after addition of $(Cu(I)(CH_3CN)_4)PF_6$) or $CuSO_4$, respectively, to the ^{15}N-labeled protein in the absence of DTT. A Jasco V-550 UV/Vis spectrophotometer was also used to monitor the binding of Cu(II) binding to apo-*Tt* Sco1.

Apo-*Tt* Cu_A was expressed and purified as described elsewhere [1] except for the affinity step which was omitted in order to avoid copper binding to the apo protein. Protein preparations showed a single band in a 14% SDS-PAGE.

Solution structure determination ---- NMR spectral assignment and structure determination were obtained through the classical triple resonance experiments using CARA software [2]. Backbone assignments were done through HNCA, HN(CO)CA, CBCA(CO)NH, HNCACB, HN(CA)CO and HNCO spectra. Side chain were assigned through 3D (h)CCH-TOCSY, HBHA(CBCACO)HN together with ^{13}C-NOESY-HSQC and ^{15}N-NOESY HSQC. The His ring protons were assigned through a ^{1}H-^{15}N HSQC experiment tailored to the detection of ^{2}J ^{1}H-^{15}N couplings and from the analysis of the ^{13}C-NOESY-HSQC spectra. Proton-proton distance constraints were derived from the analysis of 2D-NOESY, ^{15}N-NOESY-HSQC and ^{13}C-NOESY-HSQC. The secondary structure elements were predicted from the chemical shift index and angle constraints were derived accordingly. *Trans* and *cis* conformation of peptide bonds preceding prolines are identified according to chemical shift difference between Cβ and Cγ [3]. The structures were calculated using the program CYANA-2.0 [4]. The best 30 structures of the CYANA family were then subjected to restrained energy minimization (REM) with AMBER 8.0 [5]. The force field parameters for copper(I) ion and the ligands were adapted from similar systems [6,7]. The programs PROCHECK [8], PROCHECK-NMR[8 9] and WHATIF [10] were used to evaluate the quality of the structures. More than 95% of residues were located in the allowed regions of the Ramachandran plot for all structures. The conformational and energetic analyses of the structures are reported in supplemental **Tables S1-S5**. The atomic

coordinates, structural restraints and resonance assignments of apo-, Cu(I)-*Tt* PCu_AC and apo-*Tt* Sco1 have been deposited in the Protein Data Bank Resonance and BioMagResBank (PDB ID and BMRB codes, respectively: apo-*Tt* Sco1: 2k6v, 15893; apo-*Tt* PCu_AC (trans conformation): 2k6w, 15894; apo-*Tt* PCu_AC (cis conformation): 2k6y, 15895; Cu(I)-*Tt* PCu_AC (trans conformation): 2k6z, 15896; Cu(I)-*Tt* PCu_AC (cis conformation): 2k70, 15897.

Relaxation parameters measurement and data analysis ---- ^{15}N R_1, R_2, and steady-state heteronuclear ^1H–^{15}N NOEs were measured at 400 or 600 MHz NMR spectrometers using standard pulse sequences at 298K. Relaxation rates R_1 and R_2 were determined by fitting the cross-peak heights, obtained through the standard routine of Sparky software (T. D. Goddard and D. G. Kneller, University of California, San Francisco), measured as a function of the delay within the pulse sequence, to a single-exponential decay. The heteronuclear NOE values were obtained from the ratio of the peak height for ^1H-saturated and unsaturated spectra. The heteronuclear NOE values and their errors were estimated by calculating the mean ratio and the standard error from the available data sets.

EPR Spectra ---- X-band EPR spectra were acquired at 120K and 298K on a BRUKER 200D SRC EPR spectrometer.

Dissociation constant of Cu(I)-*Tt* PCu_AC and of Cu(I)-*Tt* Cu_A ---- ^{15}N-labeled Cu(I)-*Tt* PCu_AC (0.2 mM) was titrated with increasing amounts of DTT and spectral changes in the ^1H–^{15}N HSQC spectra were followed. The metallation state of Cu(I)-*Tt* PCu_AC was monitored along the NMR titration through a few residues that are spatially close to the copper(I) binding motif. Those NH cross-peaks not overlapped in the ^1H–^{15}N HSQC maps and having different chemical shifts in the apo and Cu(I) forms, were integrated during the titration steps to estimate the molar fraction of apo and copper(I) loaded forms, thus allowing the estimation of the metal affinity. The molar fractions were plotted indeed as a function of the DTT/*Tt* PCu_AC molar ratio and a conditional dissociation constant for the Cu(I)-DTT complex of 6.3×10^{-12} M at pH 7.4 and 298 K used for the K_D estimation of Cu(I)-*Tt* PCu_AC adduct. Dissociation constants of $Cu(I)_2$-*Tt* Cu_A have been similarly measured.

Protein-protein interaction ---- The interaction studies were performed in anaerobic conditions using 0.2-1.5 mM samples in 100mM potassium phosphate buffer pH 7 and followed by NMR and/or UV-visible spectroscopy. Reduced *Tt* Sco1 and *Tt* Cu_A, when appropriate, had been obtained with the addition of 5mM DTT and DTT was then removed by desalting chromatography in anaerobic chamber.

The Cys redox state of apo-*Tt* Sco1 and apo-*Tt* Cu_A, and of the protein mixtures was investigated by not-reducing SDS gel electrophoresis, after reaction with 4-acetamido-4'-maleimidylstilbene-2,2'-disulfonic acid, disodium salt (AMS) which alkylate free thiols adding a MW of ~0. 5 kDa for each reduced cyteine. Reaction of the high molecular mass thiol-conjugating agent AMS molecule with a protein allows indeed separation of two bands in the SDS gel corresponding to the two protein redox states, i.e. with two reduced thiols or with a disulphide formed. Reduced and oxidized samples and protein mixtures were treated in anaerobic environment with 1% (w/v) SDS, 10 mM AMS for 1h at 37°C and resolved by 17% not-reducing SDS-PAGE.

Supplementary data

Hydrodynamic properties of *Tt* PCu_AC and *Tt* Sco1---- The protein aggregation state of both proteins at mM concentrations was investigated by evaluating the backbone ^{15}N R_2 and R_1 relaxation properties. The correlation times for the molecular reorientation of apo- and Cu(I)-*Tt* PCu_AC and apo-*Tt* Sco1, as estimated from the R_2/R_1 ratios, are 9.0 ± 0.2, 9.2 ± 0.3 ns and 12 ± 1 ns, respectively, revealing that these proteins are monomers in solution under these conditions. No significant fast (i.e. in the ps-ns timescale) backbone mobility was observed for *Tt* PCu_AC nor for *Tt* Sco1. Only a few residues in loop 8 of apo-*Tt* Sco1 and in the solvent exposed, extended β–hairpin of both apo- and Cu(I)-*Tt* PCu_AC (those displaying line broadening above 60°C, see below), presented low ^{1}H-^{15}N heteronuclear NOE values (<0.55), indicating the presence of fast motion in the ps-ns time scale.

Spectra of apo- and Cu(I)-*Tt* PCu_AC were collected at different temperatures up to 70°C. Most amide resonances remain well dispersed up to high temperatures, without altering the observed ratio between the *trans* and *cis* forms, indicating that both the protein stability and fold are conserved at the physiological growth temperature of *Thermus thermophilus*. Resonances from a few residues (52-58, 119, 120) located in the solvent exposed, extended β–hairpin, broaden beyond detection above 60°C, indicating that this region becomes flexible at higher temperatures.

Metal binding properties of *Tt* PCu_AC, *Tt* Sco1 and *Tt* Cu_A---- In the copper(I) uptake process by *Tt* Sco1, the amide resonances of Phe41, Phe42, Gly43, Thr45, Arg46, Cys47, Val50, Leu56, Val135, His137, Ala139, Phe44, Asp49, Cys51, Thr53 and Thr54 were the most affected ones, with chemical shifts experiencing exchange in a slow to intermediate regime, which resulted in excessive broadening for some crosspeaks rendering them undetectable. These features suggest the presence of backbone conformational processes, at variance of what was found in human Sco1 and Sco2 proteins where indeed Cu(I) binding determines the formation of rigid Cu(I) complexes arising from highly flexible apo proteins. This different behavior of the Cu(I) forms can explain the lower affinity Cu(I)

site of *Tt* Sco1 with respect to human homologs.

Binding of Cu(II) ion to reduced apo-*Tt* Sco1 resulted in the appearance of absorption bands in the electronic spectrum at 356, 467 and 562 nm, with estimated absorption coefficients of 3950, 460 and 550 $M^{-1}cm^{-1}$, respectively, which level off at a 1:1 Cu(II)/protein complex (no further changes were observed beyond one equivalent). The UV-vis spectrum resembled that of the human and *B. subtilis* homologs, indicating that all Sco1 proteins bind Cu(II) in a similar fashion. The EPR spectrum of Cu(II)-Sco1 closely resembled the one obtained for *B. subtilis* Sco1 where a high affinity 1:1 Cu(II)/protein complex was also obtained.

The metal ligands of Cu_A site are His114, Cys149, Glu151, Cys153, His157 and Met160. The ^{1}H-^{15}N HSQC spectrum of the apo form of this domain exhibited several perturbations compared to the spectrum of the Cu(I) form. In particular, resonances from the sequence portions including the metal ligands (residues 111-119, and 146-162), and from residues belonging to a loop spanning residues 87–91, which is close to the copper center, were altered, as expected. Residues 126 –128 also showed smaller but still significant chemical shift perturbations (residue 126 forms a hydrogen bond with the His114 ligand). These same regions exhibited differences when the spectra of the reduced and oxidized metallated forms of *Tt* Cu_A were compared.

The Cu(I) binding affinity of *Tt* PCu_AC was estimated by NMR *via* competition with DTT. Addition of increasing amounts of DTT concentration produced a decrease in the intensity of the amide signals of Cu(I)-*Tt* PCu_AC with the concomitant formation of new resonances with chemical shifts typical of the corresponding apo form. An equilibrium constant of $(3.5 \pm 0.2)\times10^{-2}$ for the reaction involving the transfer of the Cu(I) ion from *Tt* PCu_AC to DTT was estimated and, taking into account that the K_D value for the Cu(I)-DTT complex is 6.3×10^{-12} M, the dissociation constant of Cu(I)-*Tt* PCu_AC was estimated to be $(2.2\pm 0.1) \times10^{-13}$ M. A similar approach provides a Cu(I) binding affinity of both copper ions of *Tt* Cu_A in the femtomolar range.

References

1. Slutter, C.E. *et al. Biochemistry* **35**, 3387-3695 (1996).
2. Keller, R. The Computer Aided Resonance Assignment Tutorial. CANTINA Verlag, Goldau (2004).
3. Schubert, M., Labudde, D., Oschkinat, H. & Schmieder, P. *J Biomol NMR* **24**, 149-154 (2002).
4. Guntert, P. *Methods Mol. Biol.* **278**, 353-378 (2004).
5. Case, D.A. *et al.* AMBER 8. (8.0). 2004. San Francisco, CA, University of California.
6. Banci, L. *et al. Proc. Natl. Acad. Sci. USA* **102**, 3994-3999 (2005).
7. Banci, L. *et al. Biochem. Biophys. Res. Commun.* **202**, 1088-1095 (1994).
8. Laskowski, R.A., MacArthur, M.W., Moss, D.S. & Thornton, J.M. *J. Appl. Crystallogr.* **26**, 283-291 (1993).
9. Laskowski, R.A., Rullmann, J.A.C., MacArthur, M.W., Kaptein, R. & Thornton, J.M. *J. Biomol. NMR* **8**, 477-486 (1996).
10. Vriend, G. *J. Mol. Graphics* **8**, 52-56 (1990).